Phases of frustrated quantum antiferromagnets on the square and triangular lattices

Yue Yu and Steven A. Kivelson ⓘ

Department of Physics, Stanford University, Stanford, California 94305, USA

We analyze the zero temperature phase diagrams of the spin S quantum antiferromagnet on square and triangular lattices with competing nearest and next-nearest exchange interactions as well as biquadratic couplings. We approach the problem from the large S limit. Our primary focus is on determining the extent to which the existence and character of any quantum disordered phases can be inferred from this approach.

I. INTRODUCTION

A host of interesting quantum disordered phases—including various flavors of quantum spin liquids, valence-bond solids, or quantum nematics—have by now been shown to exist as a matter of principle [1–7]. However, the issue of where they exist in the $T = 0$ phase diagram of simple models of quantum antiferromagnets with microscopically plausible interactions is still incompletely understood. Various numerical and other approaches have provided strong evidence [8–22] that there is a narrow quantum disordered regime in spin $S = 1/2$ and even $S = 1$ antiferromagnets near the point at which the classical ($S \to \infty$) model would undergo a transition from an ordered state favored by the nearest-neighbor interaction J_1 and that favored when the second-neighbor interaction, J_2 is sufficiently large [23–25].

With this physics in mind, we have studied the ground-state phase diagrams of a family of frustrated quantum antiferromagnets on the 2D square and triangular lattices. The classical $S \to \infty$ limit is readily analyzed, and indeed for all the models considered here, this analysis has been carried out previously [26]. We have extended these results by computing the leading order (and in some cases higher order) corrections to various quantities in powers of $1/S$. Much of this analysis has been carried out previously as well [27–32]. However, by extending the class of models we have considered, and by taking seriously into account the asymptotic character of the $1/S$ expansion [33], we have managed to obtain a fuller and more readily justified picture of the phase diagrams. Since for the classical pure $J_1 - J_2$ model, the transition point at $J_2 = \frac{1}{2}J_1$ is highly multicritical, we have augmented the model studied by including a weak-biquadratic interaction.

Our principle results, as we will discuss, are summarized in the schematic phase diagrams shown in Fig. 1. For the most part at large S (where our results are most reliable), instead of an intermediate quantum disordered phase, we find direct first order transitions, for instance between a Neel and stripe phase on the square lattice or the three-sublattice $120°$ antiferromagnet and the stripe phase on the triangular lattice. However, an exponentially narrow regime of a quantum disordered phase appears on the square lattice between the spin-vortex crystal (SVC) and the conical spin-vortex crystal (CSVC) phases (described in Fig. 2) and between the CSVC

and the Neel phase. On the other hand, if we extrapolate our results to smaller S, we find evidence for regimes of quantum disordered phases in the same regime of couplings suggested by earlier numerical studies, as also shown in the figure. Not reflected in the figure are a number of subtleties—including the effects of specific topological considerations associated with the quantization of S—that can alter the nature of the transitions and of the various quantum disordered phases in the phase diagrams in Fig. 1; we discuss some of these subtleties and other ambiguities in Sec. VI below.

II. THE MODEL

We considered interacting spin S operators on a regular 2D lattice, with nearest and next-nearest-neighbor quadratic interactions as well as nearest-neighbor biquadratic interactions

$$
\begin{aligned}
H = {} & \frac{1}{S^2} \sum_{\langle ij \rangle} \vec{S}_i \cdot \vec{S}_j + \frac{J_2}{S^2} \sum_{\langle\langle ik \rangle\rangle} \vec{S}_i \cdot \vec{S}_k \\
& - \frac{K}{S^4} \sum_{\langle ij \rangle} (\vec{S}_i \cdot \vec{S}_j)^2 - \frac{K'}{S^4} \sum_{\langle ijkl \rangle} (\vec{S}_i \cdot \vec{S}_j)(\vec{S}_k \cdot \vec{S}_l),
\end{aligned}
\tag{1}
$$

where $\vec{S}_j$ satisfy canonical commutation relations for spin operators, $[S_j^a, S_k^b] = i\delta_{ij}\epsilon^{abc}S_j^c$ with $\vec{S}_j \cdot \vec{S}_j = S(S+1)$. Since we will always assume that the nearest-neighbor exchange coupling, $J_1 > 0$, we can chose units of energy such that $J_1 = 1$ as in the above. We will consider explicitly the cases of a square and a triangular lattice. Here $\langle ij \rangle$ and $\langle\langle ij \rangle\rangle$ denote nearest and next-nearest neighbors, respectively, and $\langle ijkl \rangle$ signifies sites forming minimal squares on the lattice. We have normalized the interactions so that the ground-state energy density has a well defined $S \to \infty$ limit, when the spins can be treated as classical Heisenberg rotors.

For large S the effects of K and K' are very similar. For the most part, we will report explicit results for $K' = 0$, as this is slightly more convenient for the large S analysis. However, there is a significant difference for $S = 1/2$, where K can be incorporated exactly into a renormalized value of J_1, while K' remains an independent coupling constant. Thus, when extrapolating our results to $S = 1/2$, one should loosely interpret K as a proxy for K'.
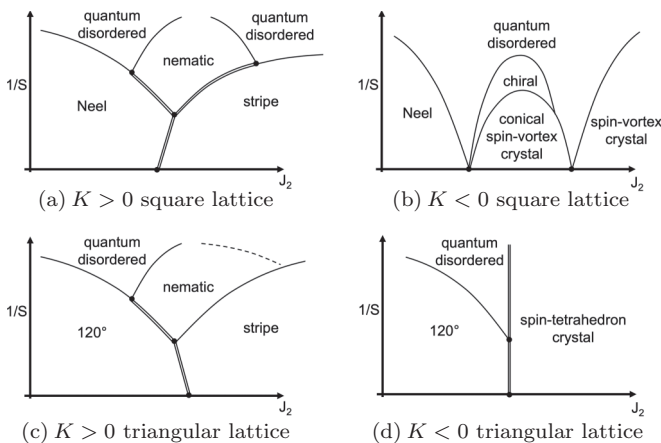
FIG. 1. Schematic ground-state phase diagrams for the square lattice spin S antiferromagnet with $K > 0$ and $K < 0$ are shown in panels (a) and (b), respectively. Panels (c) and (d) are for the triangular lattice with $K > 0$ and $K < 0$, respectively. The large S portions of the phase diagrams follow directly from the present analysis—the small S portions involve extrapolation and plausibility arguments. In the "nematic," "chiral," and "quantum disordered" phases, quantum fluctuations are sufficient to destroy magnetic long-range order, but in the first two of these we present suggestive evidence that vestigial order of the indicated variety survives from the nearby ordered phases. Moreover, in the quantum disordered phases, additional forms of order, including valence-bond crystalline and topological order may arise in ways that depend crucially on whether S is even or odd integer or half-integer.

III. CLASSICAL PHASE DIAGRAMS

A. The square lattice

The zero temperature classical phase diagram in the J_2-K plane for square lattice was discussed in Ref. [26] and is summarized in Fig. 2. When $K > 0$, there is a first order phase transition between the collinear Neel and the collinear
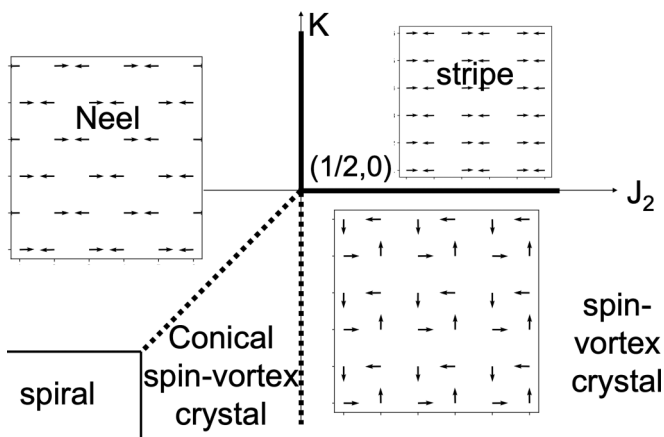
FIG. 2. Classical phase diagram for the square lattice. Collinear Neel and stripe phases are preferred by positive K. The coplanar (noncolinear) spin-vortex-crystal (SVC) and noncoplanar conical spin-vortex-crystal (CSVC) phases are preferred by negative K. In the CSVC the (spontaneously chosen) XY components of the spins order as in the SVC, and the z components exhibit Neel order.
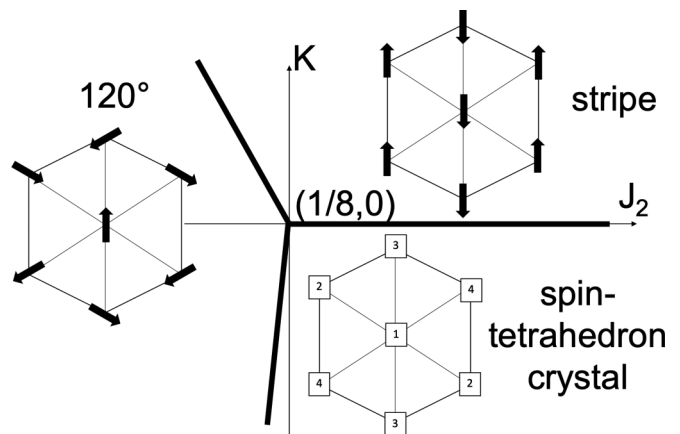
FIG. 3. Classical phase diagram for the triangular lattice. The $120°$ phase has three-sublattice coplanar spin order, and the stripe phase has two-sublattice collinear spin order, as shown in the figure. The spin-tetrahedron-crystal (STC) phase has noncoplanar order in which the spins on the four sublattices point to distinct vertices of a tetrahedron.

stripe phases at $J_2 = J_1/2$. By contrast, for $K < 0$ and of small magnitude, there are three phases as a function of increasing J_2: a Neel phase, a noncoplanar conical spin-vortex crystal (CSVC) phase, and a coplanar (noncollinear) spin-vortex crystal (SVC) phase. The SVC state, illustrated in Fig. 2, consists of alternating spin vortices on neighboring plaquettes, oriented with respect to a spontaneously chosen "X-Y" plane in spin space. The CSVC can be thought of as a linear combination of the Neel and SVC states, with spin components in the preferred X-Y plane oriented as in a SVC state, while the z components exhibit Neel-type order. It can thus be viewed as a state with coexisting Neel and SVC order, and correspondingly the two phase transitions at $J_2 = J_1/2 + K$ and $J_2 = J_1/2$ are continuous. As we will focus only on reasonably small $|K|$, we will neglect the spiral phase that arises when K is large and negative.

Note that $K = 0$ is a nongeneric line along which the classical ground states at $J_2 > J_1/2$ are highly degenerate. Here the $1/S$ analysis is subtle, involving effects of "order from disorder."

B. The triangular lattice

The zero temperature classical phase diagram in the J_2-K plane for the triangular lattice is summarized in Fig. 3. For $K > 0$ there is a first order phase transition from a $120°$ three-sublattice phase for $J_2 < \frac{J_1}{8} - \frac{9K}{16}$ to a two-sublattice stripe phase for larger J_2. For $K < 0$, the system undergoes a first order phase transition from the $120°$ phase to a four-sublattice noncoplanar spin-tetrahedron crystal (STC) phase at a critical value of $J_2 = \frac{J_1}{8} + \frac{5K}{48}$.

The $120°$ and stripe phases are shown schematically in Fig. 3. The STC has a four sublattice structure, as also shown, such that the four spins (up to a global rotation) point in the direction of the four vertices of a tetrahedron. It is easily checked that this configuration minimizes the repulsive biquadratic interaction in the four-sublattice decomposition. We will restrict attention to relatively small biquadratic

interactions K and small $|J_2 - J_1/8|$; other interesting phases could appear for stronger interactions.

IV. FIRST ORDER ($1/S$) QUANTUM CORRECTIONS

A systematic formalism for computing quantum fluctuations about the classical ground state can be accomplished using a Holstein-Primikoff (HP) transformation to map the problem into a problem of weakly interacting bosons. The first order corrections in powers of $1/S$ are obtained by keeping terms to quadratic order in the bosonic fields, i.e., treating the quantum fluctuations as noninteracting spin waves. Higher order corrections in powers of $1/S$ can be computed, in principle, by treating the interactions between bosons perturbatively. This formalism, and the details of specific calculations, are reviewed in the Appendix. In this section, we report on the quantum corrections to various quantities computed to first order in $1/S$.

The ground-state energy per lattice site of a system in a given state labeled by a (for example, $a =$ Neel) is

$$E_a = E_{cl,a} + \frac{1}{SN}\left[\sum_k \omega_{\mathbf{k},a} + C_{K,a}\right]\ldots$$
$$= E_{cl,a} + S^{-1}\mathcal{E}_a + \ldots, \quad (2)$$

where $E_{cl,a}$ is the classical ground-state energy, N is the number of sites, $\omega_{\mathbf{k},a}$ are the normal mode frequencies, $\mathbf{k}$ (which specifies the Bloch wave-number and possibly other quantum numbers where necessary) labels the individual normal modes, $C_{K,a}$ is a constant term proportional to K from $\vec{S}_i \cdot \vec{S}_i = S(S+1)$ terms in various noncollinear states, and $\ldots$ indicates higher order terms in powers of $1/S$. In particular, the noninteracting part of the HP Hamiltonian can be expressed in terms of bosonic creation operators, $b_{\mathbf{k}}^{\dagger}$, as $H_0 = \sum_{\mathbf{k}}[A_{\mathbf{k}}b_{\mathbf{k}}^{\dagger}b_{\mathbf{k}} + B_{\mathbf{k}}b_{-\mathbf{k}}^{\dagger}b_{\mathbf{k}}^{\dagger} + \text{H.c.}]$ where the coefficients $A_{\mathbf{k}}$ and $B_{\mathbf{k}}$ depend on the nature of the classical ordered state that serves as the starting point, and

$$\omega_{\mathbf{k},a} = \sqrt{|A_{\mathbf{k}}|^2 - |B_{\mathbf{k}}|^2} - A_{\mathbf{k}}. \quad (3)$$

Manifestly, this calculation only makes sense so long as $\omega_{\mathbf{k},a}$ is real for all $\mathbf{k}$, i.e., that $|A_{\mathbf{k}}|^2 - |B_{\mathbf{k}}|^2 \geqslant 0$. This is equivalent to the condition that the classical configuration be at least metastable. The specifics of the calculations of $E_{a,cl}$ and $\mathcal{E}_a$ for each of the relevant states are discussed in the Appendix.

Similarly, we will compute the anomalous expectation values of the various order parameters that characterize aspects of the broken symmetries of the various phases:

$$|\langle \mathbf{O}_a \rangle| = 1 - \mathcal{S}_a S^{-1} + \ldots, \quad (4)$$

where we will always normalize $\mathbf{O}_a$ so that the classical expectation value of its magnitude is 1, and $\mathcal{S}_a$ is a function of J_2 and K. In particular, the sublattice magnetization of the various phases is defined as

$$m_a \equiv \frac{1}{SN}\sum_{\mathbf{R}}\langle \vec{S}_{\mathbf{R}} \cdot \hat{n}_{\mathbf{R}}^{cl}\rangle, \quad (5)$$

where $\hat{n}_{\mathbf{R}}^{cl}$ is a unit vector in the direction (in spin space) of the corresponding classical orientation of spin at site $\mathbf{R}$. Again, the explicit calculations pertinent to computing $\mathcal{S}_a$ are summarized in the Appendix.

Needless to say, this expansion is strictly justified only when the corrections to the classical results are small. Where there is a first order transition, the order parameter is generally nonzero even proximate to the transition. We can determine the location of such phase boundaries by comparing the energy per site, $E_a = E_{a'}$, of the two relevant phases. Thus, the first order corrections to the position of such a phase boundary (e.g., the critical value of J_2) can be directly computed from the first order expression for the ground-state energies.

We will also make *estimates* of the points at which quantum fluctuations become sufficiently large that they cause a classical order parameter to vanish. Here we are always extrapolating our results beyond the range in which the spin-wave expansion is controlled. Moreover, since the $1/S$ expansion is known to be an asymptotic series, there is no reason to think that this estimate would be improved by keeping higher order terms in the expansion (at least without employing additional information to allow a resummation of the series). Nonetheless, it is instructive to extrapolate the results to the point at which the leading order expression for each order parameter would vanish; in this way, we interpret $\mathcal{S}_a$ as an estimate of the critical value of $S_{\text{crit}} \approx \mathcal{S}_a$ at which each of these order parameters would vanish (baring any other preemptive phase transition that destroys the order at larger S).

A. Square lattice with $K > 0$

The two pertinent phases for $K > 0$ are the Neel and the stripe phase. Both are states with nonzero sublattice magnetization, m_a, with $a =$ Neel and $a =$ str (for stripe order). The stripe phase also breaks the lattice fourfold rotational symmetry in a manner that is characterized by the nematic order parameter,

$$\langle \mathbf{O}_{\text{nem}}\rangle = \frac{1}{2NS^2}\sum_{\vec{R}}\langle \vec{S}_{\mathbf{R}} \cdot \vec{S}_{\mathbf{R}+\mathbf{x}} - \vec{S}_{\mathbf{R}} \cdot \vec{S}_{\mathbf{R}+\mathbf{y}}\rangle. \quad (6)$$

The factor of $1/2NS^2$ is included so that in the classical stripe-ordered state, $|\langle \mathbf{O}_{\text{nem}}\rangle| = 1$, so that $\mathcal{S}_{\text{nem}}$ is defined as in Eq. (4).

The first order quantum corrections to all these orders were computed previously [28]. We have added to these results expressions for the first order shifts in the ground-state energies, $\mathcal{E}_a$.

Since the classical transition between the Neel and stripe phases is first order, the $1/S$ correction to the location of the phase boundary can be computed directly by identifying the point at $E_{\text{Neel}} = E_{\text{str}}$

$$E_{\text{Neel}} - E_{\text{str}} = -2(J_1 - 2J_2) + S^{-1}[\mathcal{E}_{\text{Neel}} - \mathcal{E}_{\text{str}}] + \ldots \quad (7)$$

This is indicated by the heavy purple line in Fig. 4. Note that quantum fluctuations stabilize the Neel state relative to the stripe-ordered state. The line terminates at a value of J_2
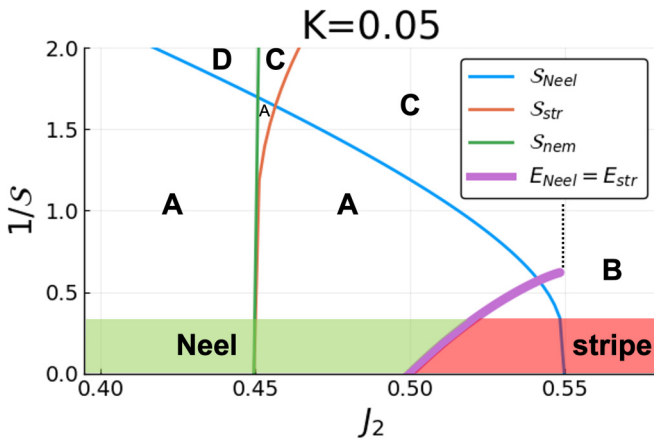
FIG. 4. First order quantum corrections to various order parameters as a function of J_2/J_1 for the square lattice with $K = 0.05$. The thick solid purple line indicates a first order boundary between the Neel and stripe phases, computed from Eq. (7). The other solid lines represent $1/\mathcal{S}_a$ for $a =$ Neel (blue), stripe (orange), and nematic (green). Interpreted as a generalized phase diagram, with $1/S$ along the y axis, the green and red regions in the large S portion of the phase diagram represent the portion that can be determined without further argument. Other regions of the phase diagram are labeled with letters for use in the discussion in Sec. V.

at which the classical Neel state ceases to be metastable; to determine the nature of the phase boundary at larger values of $1/S$ (smaller S) we will need to rely on indirect arguments, as we will discuss below. The remaining lines in Fig. 4 show the calculated values of $1/\mathcal{S}_a$ vs J_2. As is clear from the figure, for all three orders, the values of $1/\mathcal{S}_a$ vanish as $J_2 \rightarrow$ a critical value that depends on the nature of the order involved. This would seem to indicate that at this point the corresponding classical phase is unstable to quantum disordering even for arbitrary large S so long as S is not infinite. However, for large S (where our calculations are controlled) these putative quantum disordering transitions are pre-empted by the first order transition already discussed. In addition, it is worth noting that $\mathcal{S}_{\text{nem}}$ is negative for intermediate J_2 ($J_2 = 0.5$ to 0.9 at $K = 0.05$), which means first order quantum correction could enhance the nematic order. We will return to these results in Sec. V below, where we will present arguments to determine the nature of the phases in various regions labeled by letters in Fig. 4.

The K dependence of the various quantities at fixed S are shown in Fig. 5. The thin lines indicate $\mathcal{S}_a = S$ and the heavy purple line marks the point at which one would conclude $E_{\text{Neel}} = E_{\text{str}}$ from the expressions computed to first order in $1/S$. The solid lines show results for $S = 1/2$ while the dashed lines are for $S = 2$. The dashed-dotted line is where the classical Neel state starts/ends to be metastable. It is not the true boundary between nematic and stripe regime but will later be useful in Sec. V to estimate the true boundary.

B. Square lattice with $K < 0$

The relevant phases for $K < 0$ are the Neel, spin-vortex crystal (SVC), and conical spin-vortex crystal (CSVC). All are states with nonzero sublattice magnetization, m_a, with
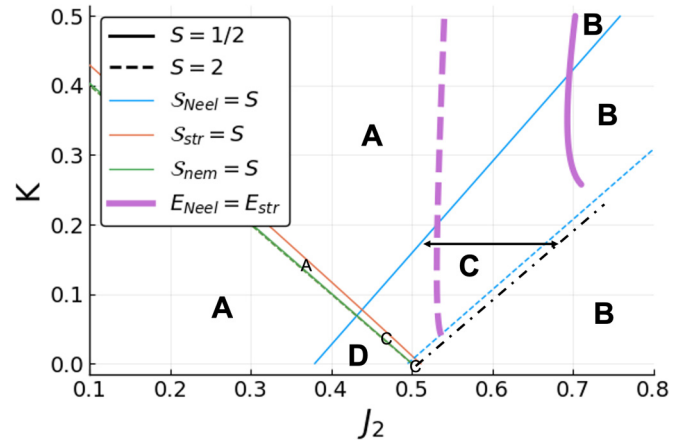
FIG. 5. Contours (thin lines) of constant $\mathcal{S}_a(J_2, K) = S$ for the square lattice with $K > 0$. The solid lines are for $S = 1/2$, and the dashed lines are for $S = 2$. The heavy purple line indicates the contour along which $E_{\text{Neel}} = E_{\text{str}}$ as computed from Eq. (7). The dashed-dotted line and letters identify different regions, as discussed in Sec. V.

$a =$ Neel, $a =$ SVC, and $a =$ CSVC. In addition, we define composite order parameters that capture specific aspects of the broken symmetry of various phases. As with the more familiar case of nematic order arising as "vestigial order [34]" upon partial melting of a stripe-ordered state, it is possible to conceive [5] of phases with vestigial broken symmetries that arise by partial melting of, respectively, a SVC or a CSVC phase such that the primary order parameter vanishes but the composite order parameters remain finite. Specifically, we define

$$\vec{\mathbf{O}}_{\text{SNVC}} \equiv \frac{1}{4NS^2} \sum_{\mathbf{R}} e^{i\mathbf{Q}\cdot\mathbf{R}} \langle \vec{S}_{\mathbf{R}+\hat{\mathbf{y}}} \times \vec{S}_{\mathbf{R}} + \vec{S}_{\mathbf{R}} \times \vec{S}_{\mathbf{R}+\hat{\mathbf{x}}}$$
$$+ \vec{S}_{\mathbf{R}+\hat{\mathbf{x}}} \times \vec{S}_{\mathbf{R}+\hat{\mathbf{x}}+\hat{\mathbf{y}}} + \vec{S}_{\mathbf{R}+\hat{\mathbf{x}}+\hat{\mathbf{y}}} \times \vec{S}_{\mathbf{R}+\hat{\mathbf{y}}} \rangle$$
$$\mathbf{O}_{\text{chir}} \equiv \frac{1}{\mathcal{N}_{\text{chir}}} \sum_{\mathbf{R}} \langle \vec{S}_{\mathbf{R}} \cdot (\vec{S}_{\mathbf{R}+\mathbf{x}} \times \vec{S}_{\mathbf{R}+\mathbf{y}}) \rangle \qquad (8)$$

which we will refer to as the spin-nematic vortex crystal (SNVC) and chiral (chir) order parameters. Here $\mathbf{Q} \equiv (\pi, \pi)$. These order parameters are, respectively, an axial vector and a pseudoscalar in spin space, both normalized so that their magnitude is 1 in a corresponding classically ordered state. A phase with $\langle \vec{\mathbf{O}}_{\text{SNVC}} \rangle \neq 0$ but $m_{\text{SVC}} = 0$ thus breaks spin-rotational order in the same sense as a spin nematic, as well as breaking translational symmetry. (From a broken symmetry perspective, it is equivalent to a triplet d-density wave [35].) A phase with $\langle \mathbf{O}_{\text{chir}} \rangle \neq 0$ but $m_{\text{CSVC}} = 0$ preserves spin-rotational and translational symmetries but has net spin chirality.

The dashed lines in Fig. 2 represent continuous transitions at $S = \infty$ between states that break distinct symmetries; since the CSVC interpolates between the Neel and the SVC phase, such transitions are in principle consistent with Landau theory. However, what is not generic is that upon approaching the transition from either side, both phases cease to be metastable (i.e., an appropriate spin-wave velocity vanishes) along the phase boundaries. Consequently, we expect that for finite $1/S$,
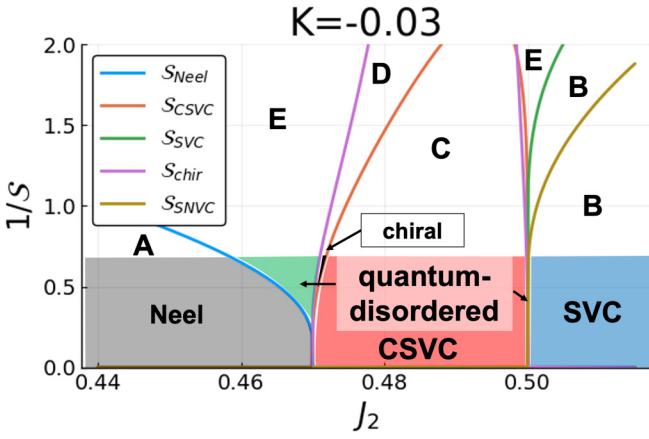
FIG. 6. First order quantum corrections to various order parameters as a function of J_2/J_1 for square lattice with $K = -0.03$. The solid lines represent $1/\mathcal{S}_a$ for $a =$ Neel (blue), conical spin-vortex crystal (orange), and spin-vortex crystal (green), as well as for $a =$ chiral (purple) and spin nematic vortex crystal (brown) phases. Interpreted as a generalized phase diagram, with $1/S$ along the y axis, the shaded regions in the large S portion of the phase diagram represent the portion of the inferred phase diagram that can be determined without further argument. Other regions of the phase diagram are labeled with letters for use in later discussions of how to interpret the results for smaller S.

FIG. 7. Contours of constant $\mathcal{S}_a(J_2, K) = 1/2$ for the square lattice with $K < 0$. The letters identify different regions discussed in Sec. V.

an intermediate region with neither form of magnetic order occurs.[1]

Indeed, as shown in Fig. 6, the curves of $1/\mathcal{S}_a$ vs J_2 for the various phases diverge from each other slowly as J_2 is tuned away from its critical value, $J_{2c}(K)$ as

$$\frac{1}{\mathcal{S}_a} \sim \frac{-G_a}{\ln|J_2 - J_{2c}|} \text{ as } |J_2 - J_{2c}| \to 0, \quad (9)$$

where in this expression $J_{2c} = J_1/2 + K$ near the convergence of the solid blue and solid orange lines (for $a =$ Neel and $a =$ CSVC) and $J_{2c} = J_1/2$ near the convergence of the solid orange and solid yellow lines (for $a =$ CSVC and $a =$ SVC). Note that for each value of a, this expression only applies as one approaches the critical value J_{2c} from the appropriate direction and that in all cases $G_a > 0$ with values that we compute explicitly in the Appendix. These results strongly suggest that, even for large S, quantum disordered phases arise near $J_2 = J_1/2 + K$ between the Neel and CSVC phases, shown as the green shaded regions in Fig. 6, and near $J_2 = J_1/2$ between the CSVC and SVC phases, which is too narrow to show up as a shaded region but is also indicated in the figure. Note that the purple line marking the contour at which the extrapolated chiral order vanishes lies inside a quantum disordered region suggesting that there are (at least) two distinct phases here—one with vestigial chiral order and one that is more fully quantum disordered. We will return to these results in Sec. V below for smaller S, where we will present

arguments to determine the nature of the phases in the various regions labeled by letters in Fig. 6.

The K dependence of the various quantities at fixed spin $S = 1/2$ are shown in Fig. 7. Solid lines indicate $\mathcal{S}_a = S$ from the expressions computed to first order in $1/S$. Classical ($S \to \infty$) phase boundaries are added as dashed lines.

C. Triangular lattice with $K > 0$

The two pertinent phases for $K > 0$ are the 120° and the stripe phase. Both are states with nonzero sublattice magnetization, m_a, with $a = 120°$ and $a =$ str (for stripe order). The stripe phase also breaks the lattice sixfold rotational symmetry in a manner that is characterized by the (three-state) nematic order parameter,

$$\mathbf{O}_{\text{nem}} \equiv \frac{1}{2NS^2} \sum_{\vec{R}} \{\langle S_{\mathbf{R}} \cdot S_{\mathbf{R}+\delta_1} \rangle$$
$$+ e^{i2\pi/3}\langle S_{\mathbf{R}} \cdot S_{\mathbf{R}+\delta_2} \rangle + e^{-i2\pi/3}\langle S_{\mathbf{R}} \cdot S_{\mathbf{R}+\delta_3} \rangle\}. \quad (10)$$

Here, $\pm\delta_i$ with $i = 1, 2$, or 3 are the unit vectors on the triangular lattice, and $\mathbf{O}_{\text{nem}} = 1$ in the classical stripe-ordered state in which the spins on site $\mathbf{R} + \delta_2$ and $\mathbf{R} + \delta_3$ have the opposite spin orientation as the spins on sites $\mathbf{R}$ and $\mathbf{R} + \delta_1$, while $\mathbf{O}_{\text{nem}} = (1 \pm i\sqrt{3})/2$ for the two other classical stripe ordered states. Like the spin vortex crystal phase in the square lattice, 120° phase also breaks the spin rotational symmetry. The vestigial phase can be characterized by the spin-nematic vortex crystal order:

$$\vec{\mathbf{O}}_{\text{SNVC}} \equiv \frac{2}{3\sqrt{3}NS^2}$$
$$\times \sum_{\triangleleft} \langle \vec{S}_1 \times \vec{S}_2 + \vec{S}_2 \times \vec{S}_3 + \vec{S}_3 \times \vec{S}_1 \rangle. \quad (11)$$

The sum is among all set of spins $(\vec{S}_1, \vec{S}_2, \vec{S}_3)$ in clockwise order (vorticity), within type A triangles ($\triangleleft$). The sum for spins also in clockwise order within type B triangles ($\triangleright$) can be shown to be exactly opposite. A phase with $\langle \vec{\mathbf{O}}_{\text{SNVC}} \rangle \neq 0$ but $m_{120°} = 0$ thus breaks spin-rotational order, but, in

---

[1]Another possibility, which is however not suggested by the spin-wave analysis, is that this transition could be replaced by a fluctuation driven first order transition.
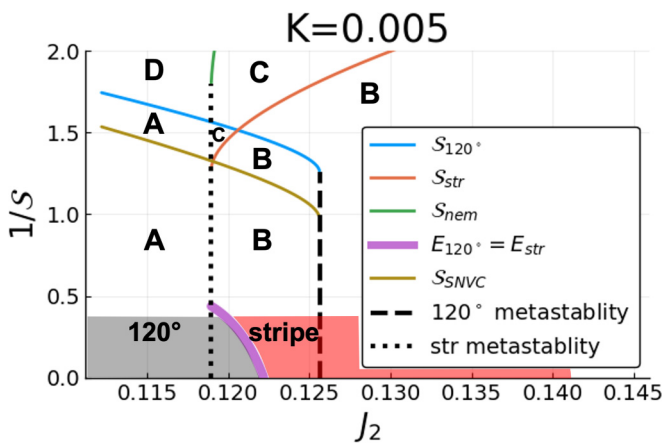
FIG. 8. First order quantum corrections to various order parameters as a function of J_2/J_1 for triangular lattice with $K = 0.003$. The thick solid purple line indicates a first order boundary between the 120° and stripe phases, computed from Eq. (12). The other solid lines represent $1/\mathcal{S}_a$ for $a = 120°$ (blue), stripe (orange), SNVC (brown), and nematic (green). Interpreted as a generalized phase diagram, with $1/S$ along the y axis, the gray and red regions in the large S portion of the phase diagram represent the portion of the inferred phase diagram that can be determined without further argument. Other regions of the phase diagram are labeled with letters for use in later discussions of how to interpret the results for smaller S.

contrast with the SNVC phase on the square lattice, it does not break translational symmetry.

Since the classical transition between the 120° and stripe phase is first order, the $1/S$ correction to the location of the phase boundary can be computed directly by identifying the point at $E_{120°} = E_{\text{str}}$

$$E_{120°} - E_{\text{str}} = -0.5(J_1 - 8J_2) + S^{-1}[\mathcal{E}_{120°} - \mathcal{E}_{\text{str}}] + \ldots \tag{12}$$

This is indicated by the heavy purple line in Fig. 8. Note that quantum fluctuations stabilize the stripe state relative to the 120° state. The line terminates at a value of J_2 at which the classical stripe state ceases to be metastable; the remaining lines in Fig. 8 show the calculated values of $1/\mathcal{S}_a$ vs J_2. As is clear from the figure, for all four orders, $1/\mathcal{S}_a$ approaches nonzero values as $J_2 \to$ a critical value that depends on the nature of the order involved.

The K dependence of the various quantities at fixed S are shown in Fig. 9. Representative of the large spin case, the line in the K-J_2 plane along which $E_{120°} = E_{\text{str}}$ for $S = 5$ is marked by the heavy dashed purple line; no solution of this equation exists in the small spin case, $S = 1/2$. Conversely, the lines on which $\mathcal{S}_a = S$ in the small spin case, $S = 1/2$, are marked by the thin solid lines; no such lines exist at large spin $S = 5$.

D. Triangular lattice with $K < 0$

The two pertinent phases for $K < 0$ are the 120° and the spin-tetrahedron crystal phase. Both are states with nonzero sublattice magnetization, m_a, with $a = 120°$ and $a = $ STC (for spin-tetrahedron crystal order).

Since the classical transition between the 120° and STC phase is first order, the $1/S$ correction to the location of the
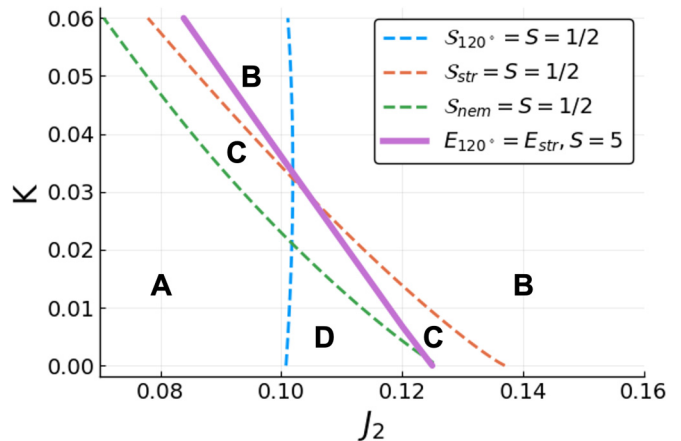
FIG. 9. Contours of constant $\mathcal{S}_a(J_2, K) = S$, as dashed lines for $S = 1/2$. The solid heavy purple line indicates the contour along which $E_{120°} = E_{\text{str}}$ as computed from Eq. (12), for $S = 5$. The letters identify different regions, as discussed in Sec. V.

phase boundary can be computed directly by identifying the point at which $E_{120°} = E_{\text{STC}}$. In the classical $S \to \infty$ limit, this occurs at the limit of metastability of the 120° phase. Moreover, in the entire regime in which both states are classically metastable, the 120° phase always has a lower energy even when first order quantum corrections are included. Thus, this first order phase boundary does not vary with S to first order in $1/S$; the first order boundary between 120° phase and STC phases occurs at $J_2 = \frac{J_1}{8} + \frac{K}{8}$ in Fig. 10.

The K dependence of the various quantities at fixed spin $S = 1/2$ are shown in Fig. 11. Thin solid lines indicate $\mathcal{S}_a = S$ from the expressions computed to first order in $1/S$.
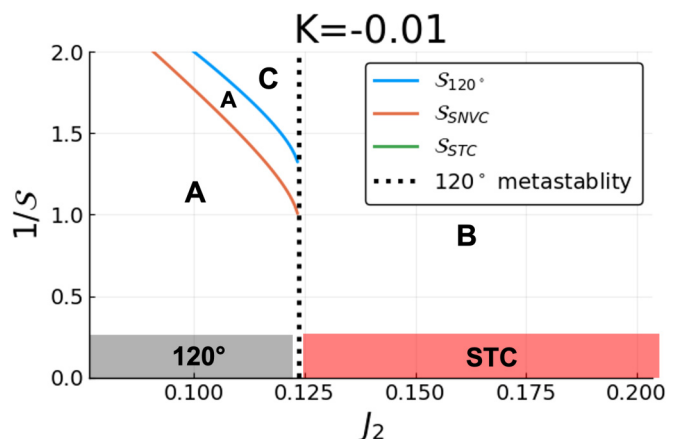
FIG. 10. Phase diagram in the J_2/J_1-$1/S$ plane, for $K = -0.01$. The solid lines represent $1/\mathcal{S}_a$ for $a = 120°$ (blue), SNVC (orange), and STC phase (above $S = 1/2$ boundary). The shaded regions in the large S portion of the phase diagram represent the portion of the inferred phase diagram that can be determined without further argument. Other regions of the phase diagram are labeled with letters for use in later discussions of how to interpret the results for smaller S.
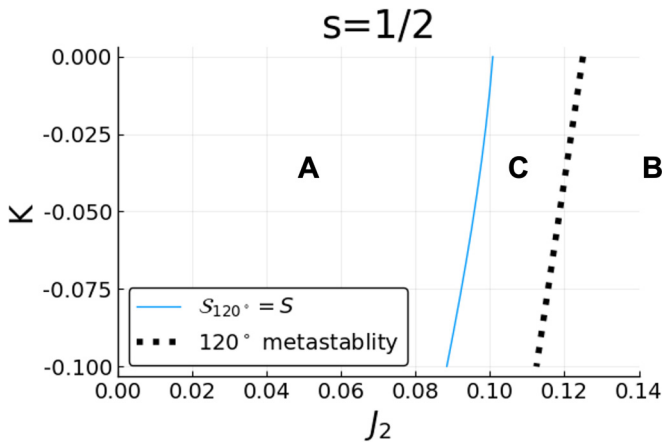
FIG. 11. Contours of constant $\mathcal{S}_a(J_2, K) = S$, for $S = 1/2$. The letters identify different regions discussed in Sec. V. Black line is where $120°$ phase ceases to be metastable.

V. EXTRAPOLATION TO SMALLER S

While there are surely dangers involved, it is worthwhile extrapolating the results that are controlled at large S to form at least a conjectural completion of the phase diagrams, as shown in Fig. 1. This also allows us to make contact with a host of numerical studies that have been performed on the same models for the cases of $S = 1/2$ and $S = 1$. In this section, we outline the logic that leads to this figure. In all cases, when we refer to "the ground state energy" or "the magnitude of the order parameter" we are implicitly referred to quantities that are computed to leading order in $1/S$. For example, when we refer to a region of the phase diagram in which the Neel order parameter vanishes, we mean a region where $S < \mathcal{S}_{\text{Neel}}$, i.e., where the extrapolated magnitude of the order parameter would be negative.

A. Square lattice with $K > 0$

Our analysis of the square lattice with $K > 0$ is based on identifying the nature of the ground state in the various regions shown in Fig. 4 which are labelled by different letters. Everywhere to the left of the solid purple line (i.e., regions A, C, and D) the energy of the Neel state is lower than the stripe phase, implying that the stripe phase is excluded in all these regions. In region A (i.e., below the blue line) the magnitude of m_{Neel} is positive, so we identify this as being approximately the region in which Neel order survives quantum fluctuations.

Conversely, in regions C and D, m_{Neel} vanishes, which we interpret as meaning that no magnetic order survives in either region. Indeed, in region D all the orders we have considered are precluded, so we identify it as a fully quantum disordered regime. On the other hand, in region C quantum fluctuations of the nematic order do not cause it to vanish, so we conjecture that this corresponds to a nematic phase. Similarly all of region (B) is likely stripe ordered, since the stripe state is energetically preferred, and its order parameter including first order quantum corrections is nonzero.

The nature of phase transitions can now be considered. The transition indicated by the heavy purple line in Fig. 4 between the Neel and stripe phases is first order and is unambiguously

calculable when S is large. Since we have identified the phase transitions between different regions separated by thin solid lines as the points at which quantum fluctuations become large enough that one or another order parameter vanishes, we have implicitly assumed that these transitions are all continuous. For the cases of the Neel to disordered (A to D) and the nematic to disordered (C to D), these correspond to reasonable Landau-allowed order to disorder transitions. However, the implied Neel to nematic transition (A to C) is not Landau allowed, and indeed to the extent that the first order in $1/S$ expressions can be trusted, the nematic order would have a finite jump across this transition. While, as discussed in Sec. VI, under special conditions, a "beyond Landau" continuous deconfined quantum critical transition [36] between a Neel and a quantum nematic paramagnet is possible [2], far more likely is that the transition between these two phases is first order and probably not quite at the same point as the solid blue line.

The nature of the phase transition between the nematic and stripe phases is also unclear. This is Landau allowed to be continuous although at least where it occurs along the heavy purple line it is probably first order. If we were to extend the range of parameters shown in Fig. 4 we would find that the orange line $1/\mathcal{S}_{\text{str}}$ and the green line $1/\mathcal{S}_{\text{nem}}$ cross at $J_2 \approx 3J_1$; we interpret this crossing as a bicritical point marking the end of the first order stripe to nematic phase boundary, beyond which a direct stripe to quantum disordered transition is expected.

The K dependence of the phase diagram can be obtained from the same sort of analysis. Contours of $\mathcal{S}_a = S$ and lines of $E_a = E_b$ in Fig. 5 are now used to estimate the phase boundaries. Phases (A) Neel, (B) stripe, (C) nematic, and (D) quantum disordered are explicitly labeled for $S = 1/2$. For small K, the width of the "nematiclike" phase (C), and of the quantum disordered phase (D)—indicated by the black arrow between blue and dashed-dotted line in the main panel of Fig. 5)—become exponentially small as S increases, and so are invisible for $S = 2$. Together, these considerations lead to the schematic phase diagram shown in Fig. 1(a).

B. Square lattice with $K < 0$

For the square lattice with $K < 0$, the analysis that leads from Figs. 6 and 7 to the schematic phase diagram in Fig. 1(b) is relatively straightforward. Specifically, as can be seen in Fig. 6, the basic topology of the phase diagram is already established when S is large and hence can be interpreted without need of extrapolating to smaller S. Thus regions A, B, C, D, and E correspond to Neel, SVC, CSVC, chiral, and quantum disordered phases, respectively.

The nature of phase transitions can now be considered. Again, since we have identified the phase transitions as the points at which quantum fluctuations become large enough that one or another order parameter vanishes, we have implicitly assumed that these transitions are all continuous. All the phase transitions here are Landau allowed to be continuous. The K-dependence phase diagram can be obtained from the same sort of analysis. In common with the $K > 0$ case, the width of the quantum disordered phase (E), and of the chiral phase (D)—indicated by black arrow in Fig. 7—decreases

exponentially as S increases. However, one noticeable difference is that the quantum disordered regime is present even at large $|K|$ in the phase diagram with $K < 0$. Note that both CSVC and chiral phases requires sufficiently large $|K|$ to develop nonzero order parameters. Therefore, at small $|K|$, the width of quantum disordered phase increase as $|K|$ increases. This can be traced back to the fact that "order by disorder" phenomena [23] effectively add [37] a positive contribution to K which tends to stabilize the two collinear states (Neel and stripe). These considerations lead to the schematic phase diagram shown in Fig. 1(b), in which phase boundary between chiral and CSVC phase have been extended and connected to larger $1/S$ for artistic reasons.

C. Triangular lattice with $K > 0$

The schematic phase diagram for the triangular lattice with $K > 0$ shown in Fig. 1(c) is obtained by identifying the most likely phase corresponding to the different labeled regions in Figs. 8 and 9 which are labeled by different letters. Everywhere to the left of the solid purple line in Fig. 8 (i.e., regions A and D) the energy (where it can be computed) of the 120° state is lower than that of the stripe phase, implying that the stripe phase is excluded. In region A (i.e., below the blue line) the magnitude of $m_{120°}$ is positive, so we identify this as the region in which 120° order survives quantum fluctuations. However, in regions D, $m_{120°}$ vanishes, which we interpret as meaning that no magnetic order survives in this region. Indeed, in region D all the orders we have considered are precluded, so we identify it as a fully quantum disordered regime. Similarly all of region B is likely stripe ordered, since the stripe state is energetically preferred, and its order parameter including first order quantum corrections is nonzero. In region C, the nematic order does not vanish, while stripe order vanishes and $m_{120°}$ phase is energetically excluded; so we conjecture that this corresponds to a nematic phase.

The nature of phase transitions can now be considered. The analysis closely parallels that of the square lattice with $K > 0$. The transition indicated by the heavy purple line in Fig. 8 between the $m_{120°}$ and stripe phases is first order and is unambiguously calculable when S is large. Since we have identified the phase transitions between different regions separated by thin solid lines as the points at which quantum fluctuations become large enough that one or another order parameter vanishes, we have implicitly assumed that these transitions are all continuous. For the cases of the $m_{120°}$ to disordered (A to D) and the nematic to disordered (C to D), these correspond to reasonable Landau-allowed order to disorder transitions. However, the implied $m_{120°}$ to nematic transition (A to C) is not Landau allowed, and indeed to the extent that the first order in $1/S$ expressions can be trusted, the nematic order would have a finite jump across this transition. It is thus likely that the transition between these two phases is first order and probably not quite at the same point as the solid blue line. The nature of the phase transition between nematic and stripe phase is also unclear. This is Landau allowed to be continuous. Different from square lattice, we are unable to extend the range of parameters shown in Fig. 8 to larger J_2, since there are other relevant phases. Thus, we are unable to

confirm the existence of a bicritical point marking the end of the first order stripe to nematic phase boundary, beyond which a direct stripe to quantum disordered transition is expected.

The K dependence of the phase diagram can be obtained from the same sort of analysis. Contours of $\mathcal{S}_a = S$ for $S = 1/2$ (dashed lines) and line of $E_a = E_b$ for $S = 5$ (solid line) in Fig. 9 are now used to estimate the phase boundaries. Phases (A) 120°, (B) stripe, (C) nematiclike, and (D) quantum disordered are explicitly labeled for $S = 1/2$. Contrary to the results of the square lattice, since quantum correction $\mathcal{S}$ to order parameter does not have the logarithmic divergence as J_2 approaches the critical value $J_1/8$, the width of the nematic and quantum disordered phase does not decay exponentially as S increases. It has been shown in Fig. 8 that these two phases do not appear at large spin.

D. Triangular lattice with $K < 0$

Finally, we use the results in Figs. 10 and Fig. 11 to construct the qualitative phase diagram for the triangular lattice with $K < 0$ shown in Fig. 1(d). It should be noted that the solid line in Fig. 10 indicating the value of $1/\mathcal{S}_a$ for $a = $ STC is not shown since $1/\mathcal{S}_{\text{STC}} > 2$ corresponding to an unphysical value of $S < 1/2$. For region A under the blue line the 120° order parameter is apparently nonzero. We thus identify region A with the 120° phase. Region B is identified with the STC phase, since only the STC state is metastable, and its order parameter is estimated to be nonzero. Region C is not in the 120° nor the STC phase, since the 120° order parameter vanishes, and the STC state has a higher energy than the 120° state. It may be in a quantum disordered phase, or another symmetry breaking vestigial phases that we have not considered. The K-dependence phase diagram at fixed $S = 1/2$ is summarized in Fig. 11. As is the case with the square lattice, quantum fluctuations tend to stabilize the positive K phases relative to those with negative K as a form of order from disorder.

The phase boundaries are now given by two lines. One is the blue line for $1/\mathcal{S}_{120°}$ in Fig. 10 that separates the 120° phase and the quantum disordered phase. Another one is at $J_2 = \frac{J_1}{8} + \frac{K}{8}$, where the classical 120° state ceases to be metastable, that separates STC phase with other two phases. The phase transition between the 120° phase and the quantum disordered phase should be continuous, since the order parameter $\mathbf{O}_{120°}$ vanishes continuously upon approaching the phase boundary. The phase transitions between STC phase and the other two phases (120° and quantum disordered phase) should be first order, since the STC order parameter $\mathbf{O}_{\text{STC}}$ is nonzero upon approaching the phase boundaries.

E. Comments on the structure of the $1/S$ expansion

Based on the above extrapolation of the first order in $1/S$ expansion to smaller S, we obtained the schematic phase diagrams in Fig. 1. As stated in the beginning of this section, the extrapolation is dangerous and its validity cannot be guaranteed. However, in this subsection, we would like to comment on the validity of this extrapolation, by comparing the results of the first order $1/S$ expansion with the second order $1/S$ expansion. Since the $1/S$ expansion is an
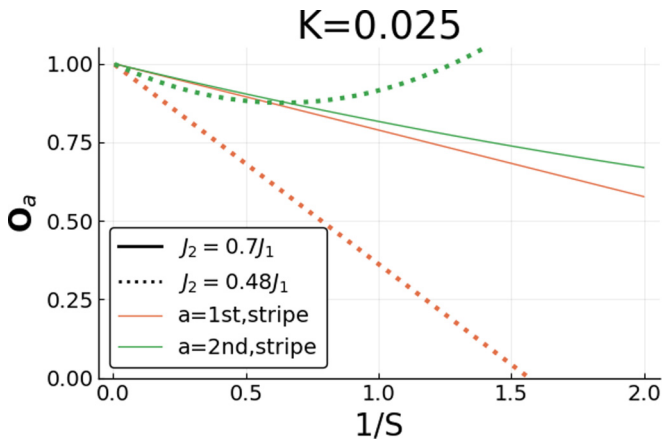
FIG. 12. Stripe order parameter $\mathbf{O}_{str}$, calculated from first and second quantum correction as a function of $1/S$. Solid lines are for $J_2 = 0.7J_1$, and dashed lines are for $J_2 = 0.48J_1$, under the same K.

asymptotic series [33], where the first and second order results differ substantially, it is far from clear which is closer to the correct answer. Therefore, this comparison only functions as a "comment" rather than any systematic proof of the validity of the above extrapolations.

For illustration purpose, we only focus on the stability of the stripe phase on the square lattice with $K > 0$. This has been calculated in Ref. [38], for the case without a biquadratic interaction. In general, the biquadratic interaction can be approximated by the following quadratic interaction.

$$(S_i \cdot S_j)^2 \approx [2(S_i \cdot S_j)\langle S_i \cdot S_j\rangle - \langle S_i \cdot S_j\rangle^2], \quad (13)$$

and if the classical configuration is collinear, $\langle S_i \cdot S_j\rangle$ can then be replaced by its classical expectation value. For the stripe phase, the above mean-field approximation leads an anisotropic term, which has already been included in the previous study [38].

As a function of $1/S$, the stripe order parameter $\mathbf{O}_{str}$ under first order (orange line) and second order (green line) $1/S$ expansion are plotted in Fig. 12. Solid lines are for $J_2 = 0.7J_1$, and dashed lines are for $J_2 = 0.5J_1$. As $1/S$ grows, the second order results start deviating from the first order quantum correction. The first order result on $\mathbf{O}_a$ should not be trusted if the deviation is big. Therefore, as $J_2 \to J_1/2 - K$, the order parameter $\mathbf{O}_a$ from first order quantum correction becomes trustable only at large spin.

In our previous extrapolations, we use $\mathcal{S}$ to estimate the true phase boundary $\mathcal{S}_{crit}$. This estimation in general works better at larger spin and further away from the critical point.

VI. BEYOND SPIN-WAVE ANALYSIS

There are a large number of additional subtleties that we have overlooked in the present analysis. We have treated $1/S$ as a continuous parameter that tunes the extent of the quantum oscillations—this is very similar in spirit to the classic approach of Ref. [39]. However, S is in fact a discrete variable, and there can be differences in the physics depending on whether it is integer or half-integer [40–42] and even whether it is an even integer or an odd integer [2,43]. This can effect the

nature of the allowed phases and opens up the possibility of exotic, beyond Landau deconfined quantum phase transitions [36]. For instance, generalizations of the famous Lieb-Schulz-Mattis theorem [44–46] imply that the disordered phase for a half-integer spin must either have a broken symmetry (e.g., exhibit valence-bond-crystalline order) or be one or another of quantum spin liquid with topological order.

Since most of the numerical studies to date have been carried out for $S = 1/2$, or, to a lesser extent, for $S = 1$, these additional subtleties are likely to be significant. However, we can still distinguish magnetically ordered phases from quantum disordered phases. Moreover, within the regime of quantum disordered phases, we may be able to distinguish those that exhibit broken symmetries as a form of vestigial order, if the order is accompanied by reasonably long but still finite range correlations that reflect the structure of a nearby magnetically order, vs broken symmetries (such as the before mentioned topological order) that are more readily identified with topological terms in the effective field theory [42], rather than with any proximate magnetically ordered state.

Intense effort and enormous creativity has been marshaled for the numerical search for intermediate nonmagnetic quantum-disordered states in the $J_1 - J_2$ models (with $K = 0$). For $S = 1/2$ on the square [9–18] and triangular lattice [19–22], various numerical works have confirmed the existence of intermediate quantum disordered states. However, the nature of the intermediate state(s) is still under debate. For $S = 1$ on a square lattice, there is contradictory evidence concerning the existence of intermediate phases [8,47,48]; notably, in the study [8] that is most strongly indicative of the occurrence of such a phase, it is found to occur in an exceedingly narrow range of J_2 and to have a clear nematic character. We are unaware of any studies of the $S = 1$ model on the triangular lattice. Since finite S effectively adds a positive K, one should compare the above numerical studies
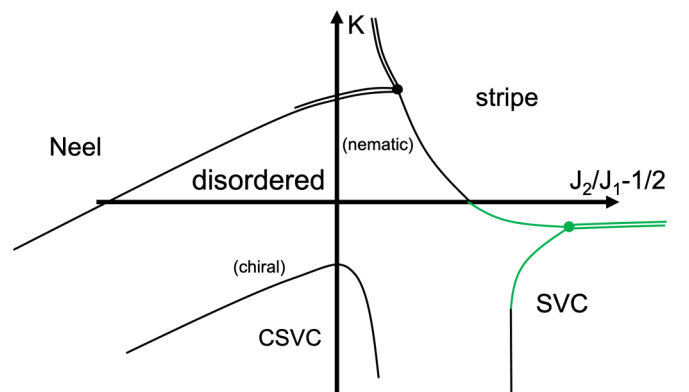
FIG. 13. Schematic phase diagram for the square lattice in the J_2-K plane, representative of the expected behavior with a fixed small value of S. All results are based on speculative extrapolations made on the basis of the large S results. The results suggest that negative K is likely to enhance the range of stability of various quantum disordered phases. Double solid lines denote the first-order phase transitions. Black lines are imported from Figs. 5 and 7, and green lines are reasonable continuations. Some forms of vestigial order that may persist within the quantum disordered regime are indicated in parentheses.

with the phase diagrams in our work with $K > 0$. At least in terms of the general topology of the phase diagram, the results of the existing numerical studies appear to be consistent with those shown in Figs. 1(a) and 1(c).

An interesting future direction for numerical studies suggested by the present study is to investigate the model with negative K (or K' for $S = 1/2$) where the quantum disordered phases are found to persist to large S and to have a broader region of stability. Based on the speculative extension of our previous discussion to some fixed small S, a schematic phase diagram in the J_2-K plane for the square lattice is shown in Fig. 13.

VII. CONCLUSION

We have analyzed the Heisenberg antiferromagnet at $T = 0$ on square and triangular lattice with nearest neighbor and next-nearest neighbor quadratic interactions, and nearest-neighbor biquadratic interactions using linear spin wave theory. At large S (where the results are most readily justified) we found that the classical first order transition between the Neel and stripe phase is stable. However, the classical continuous phase transitions involving various noncolinear magnetic phases are eliminated, even at large S, and are replaced by intermediate quantum disordered phases. Our results indicate new regimes to search for quantum disordered phases in future numerical work.

APPENDIX A: HOLSTEIN-PRIMAKOFF TRANSFORMATION FOR COPLANAR (INCLUDING COLLINEAR) CONFIGURATION

In this section, we would like to review a systematic way to perform Holstein-Primakoff transformation, if the classical configuration is coplanar. This will eventually lead to a translational invariant Hamiltonian, in terms of creation and annihilation operators, for Neel, stripe, and SVC state. Without loss of generality, let us suppose spins in the classical configuration are in the xz plane $\vec{n}_i = (\sin\theta_i, 0, \cos\theta_i)$.

If $\theta = 0$, the standard Holstein-Primakoff transformation is

$$(J_{x0}, J_{y0}, J_{z0}) = (\sqrt{2S}\frac{b + b^\dagger}{2}, \sqrt{2S}\frac{b - b^\dagger}{2i}, S - b^\dagger b). \tag{A1}$$

Here, we have already taken the leading order contribution in HP transformation. Generally, for arbitrary θ_i, we can choose

$$
\begin{aligned}
J_x &= J_{x0}\cos\theta_i + J_{z0}\sin\theta_i \\
J_y &= J_{y0} \\
J_z &= J_{z0}\cos\theta_i - J_{x0}\sin\theta_i.
\end{aligned} \tag{A2}
$$

Now we would like to explicitly write down $\vec{J}_i \cdot \vec{J}_j$, up to quadratic terms in terms of bosonic operators. The constant term $\vec{J}_i \cdot \vec{J}_j$ is $S^2\cos\theta$ if J_i and J_j are different spin, and $S(S+1)$ if $i = j$. This will be important when calculating ground state energy. The linear terms in $\vec{J}_i \cdot \vec{J}_j$ are

$$\frac{1}{S}(\vec{J}_i \cdot \vec{J}_j)_{\text{linear}} = \frac{\sin\theta}{\sqrt{2}}(b_i + b_i^\dagger - b_j - b_j^\dagger), \tag{A3}$$

which is useful in the biquadratic interaction $(\vec{J}_i \cdot \vec{J}_j)^2$, which contains the square of the above linear terms. The quadratic terms in $\vec{J}_i \cdot \vec{J}_j$ are

$$\frac{1}{S}(\vec{J}_i \cdot \vec{J}_j)_{\text{quadratic}} = -(b_i^\dagger b_i + b_j^\dagger b_j)\cos\theta + \frac{1}{2}(1 + \cos\theta)(b_i^\dagger b_j + \text{c.c.}) + \frac{1}{2}(-1 + \cos\theta)(b_i^\dagger b_j^\dagger + \text{c.c.}). \tag{A4}$$

θ is the angle difference between i and j in the classical configuration.

For the coplanar Neel, stripe, and SVC phase, $\cos\theta$ and $\sin^2\theta$ for nearest neighbored and next-nearest neighbored spins is invariant under translation. Therefore, a translational invariant Hamiltonian in terms of creation and annihilation operators is expected.

In the next subsections, we will explicitly derive the resulted Hamiltonian for the Neel and stripe phase. We will include the result for the SVC phase.

1. Square lattice-Neel and stripe phase

In this section, we consider the general ordering vector $\vec{Q} = (\pi, \theta)$, $\theta = 0, \pi$, which describes the Neel-stripe transition. For the nearest neighbored J_1 terms, angle difference is $\pm\pi$ along the x direction and $\pm\theta$ along the y direction. Plugging in the

Holstein-Primakoff transformation in Eq. (A4), we get

$$(J_1/S) \times \left[\sum_i 2(1 - \cos\theta) b_i^\dagger b_i + \sum_{\langle ij \rangle Y} \frac{1}{2}(1 + \cos\theta)(b_i^\dagger b_j + \text{c.c.}) + \sum_{\langle ij \rangle Y} \frac{1}{2}(-1 + \cos\theta)(b_i^\dagger b_j^\dagger + \text{c.c.}) + \sum_{\langle ij \rangle X}(-1)(b_i^\dagger b_j^\dagger + \text{c.c.}) \right]$$

(A5)

Note that the summation along x and y are separately written down. For second nearest neighbored J_2 terms, the angle difference is $\pm(\pi \pm \theta)$. After Holstein-Primakoff transformation, we have

$$(J_2/S) \times \left[\sum_i 4\cos\theta\, b_i^\dagger b_i + \sum_{\langle\langle ij \rangle\rangle} \frac{1}{2}(1 - \cos\theta)(b_i^\dagger b_j + \text{c.c.}) + \sum_{\langle\langle ij \rangle\rangle} \frac{1}{2}(-1 - \cos\theta)(b_i^\dagger b_j + \text{c.c.}) \right].$$

(A6)

For the biquadratic terms, we first perform mean-field approximation and then Holstein-Primakoff transformation:

$$-K/S^4 \sum_{\langle ij \rangle}(\vec{J}_i \cdot \vec{J}_j)^2 = 2K/S^2 \sum_{\langle ij \rangle_x} \vec{J}_i \cdot \vec{J}_j - 2K/S^2 \cos\theta \sum_{\langle ij \rangle_Y} \vec{J}_i \cdot \vec{J}_j - KN(1 + \cos^2\theta)$$

$$= (2K/S) \times \left[\sum_i 2(1 + \cos^2\theta) b_i^\dagger b_i + \sum_{\langle ij \rangle Y} \frac{1}{2}(-1 - \cos\theta)\cos\theta(b_i^\dagger b_j + \text{c.c.}) \right.$$

$$\left. + \sum_{\langle ij \rangle Y} \frac{1}{2}(1 - \cos\theta)\cos\theta(b_i^\dagger b_j^\dagger + \text{c.c.}) + \sum_{\langle ij \rangle X}(-1)(b_i^\dagger b_j^\dagger + \text{c.c.}) \right] - KN(1 + \cos^2\theta).$$

(A7)

N is the total number of sites.

Now we can perform Fourier transformation

$$b_i^\dagger = \frac{1}{\sqrt{N}} \sum_{\vec{k}} e^{i\vec{k} \cdot \mathbf{R_i}} b_{\vec{k}}^\dagger.$$

(A8)

Dropping the constant terms, we have

$$H = \frac{1}{S} \sum_{\vec{k}} A_k(b_k^\dagger b_k + b_{-k}^\dagger b_{-k}) + B_k(b_k^\dagger b_{-k}^\dagger + b_k b_{-k})$$

$$A_k = [(1 - \cos\theta) + \frac{1}{2}(\cos\theta + 1)\cos k_y]J_1 + [2\cos\theta + (1 - \cos\theta)\cos k_x \cos k_y]J_2$$

$$+ \left[(1 + \cos^2\theta) + \frac{1}{2}(-\cos\theta - 1)\cos\theta \cos k_y \right](2K)$$

(A9)

$$B_k = \left[\frac{1}{2}(\cos\theta - 1)\cos k_y - \cos k_x \right]J_1 + (-1 - \cos\theta)\cos k_x \cos k_y J_2$$

$$+ \left[\frac{1}{2}(-\cos\theta + 1)\cos\theta \cos k_y - \cos k_x \right](2K).$$

By taking $\theta = 0, \pi$, we can reproduce the result for the stripe and Neel phase, as obtained in Ref. [28].

2. Square lattice-SVC phase

In the classical configuration for the SVC state, the angle between nearest neighbors is $\pi/2$, and the angle difference between next-nearest neighbors is π. The Hamiltonian in terms of bosonic operators is

$$H = \frac{1}{S} \sum_{\vec{k}} A_k(b_k^\dagger b_k + b_{-k}^\dagger b_{-k}) + B_k(b_k^\dagger b_{-k}^\dagger + b_k b_{-k}) + \text{const.}$$

$$A_k = \frac{J_1}{2}(\cos k_x + \cos k_y) + 2J_2 - K(2 - \cos k_x - \cos k_y)$$

$$B_k = -\frac{J_1}{2}(\cos k_x + \cos k_y) - 2J_2 \cos k_x \cos k_y - K(2 - \cos k_x - \cos k_y).$$

(A10)

3. Triangular lattice-120° phase and stripe phase

In this section, we will apply Holstein-Primakoff transformation to the coplanar 120° phase and stripe phase. We will explicitly derive the 120° phase, while providing the result for the stripe phase.

For 120° phase, the angle difference is 120° for all nearest neighbors. Plugging in the Holstein-Primakoff transformation, we get

$$(J_1/S) \times \left[\sum_i 3b_i^\dagger b_i + \sum_{\langle ij \rangle} \frac{1}{4}(b_i^\dagger b_j + \text{c.c.}) + \sum_{\langle ij} -\frac{3}{4}(b_i^\dagger b_j^\dagger + \text{c.c.}) \right]. \tag{A11}$$

For the next-nearest neighbored J_2 terms, angle difference is $0°$, that leads to

$$(J_2/S) \times \left[\sum_i -6b_i^\dagger b_i + \sum_{\langle ij \rangle} (b_i^\dagger b_j + \text{c.c.}) \right]. \tag{A12}$$

Biquadratic terms can be treated by performing mean-field approximation. Firstly, similar to the derivation of Neel phase for square lattice, it effectively modifies the nearest neighbor coupling constant J_1 as follows:

$$J_1 \to J_1 - 2K/S^2 \langle J_i \cdot J_j \rangle = J_1 + K. \tag{A13}$$

Secondly, since the configuration is not collinear, there is an extra term from the square of the linear term in HP transformation

$$-K \sin^2 120° \sum_{\langle ij \rangle} (J_{i,x0} - J_{j,x0})^2. \tag{A14}$$

After performing Fourier transformation, the final result for 120° phase is

$$H = E_{cl} + \frac{1}{S} \sum_{\vec{k}} A_k(b_k^\dagger b_k + b_{-k}^\dagger b_{-k}) + B_k(b_k^\dagger b_{-k}^\dagger + b_k b_{-k}) - \frac{9KN}{8S}$$

$$A_k = (J_1 + K)\left[\frac{3}{2}\left(1 + \frac{1}{2}\gamma_k\right) \right] + J_2(-3 + 3\gamma_k') - \frac{9K}{4}(1 - \gamma_k)$$

$$B_k = (J_1 + K)\left(-\frac{9}{4}\gamma_k\right) - \frac{9K}{4}(1 - \gamma_k)$$

$$\gamma_k = \frac{1}{6}\sum_{\vec{\delta}_1} \exp(i\vec{k}\cdot\vec{\delta}_1) = \frac{1}{3}\left(\cos k_y + 2\cos\frac{\sqrt{3}k_x}{2}\cos\frac{k_y}{2}\right)$$

$$\gamma_k' = \frac{1}{6}\sum_{\vec{\delta}_2} \exp(i\vec{k}\cdot\vec{\delta}_2) = \frac{1}{3}\left(\cos\sqrt{3}k_x + 2\cos\frac{\sqrt{3}k_x}{2}\cos\frac{3k_y}{2}\right).$$

The final result for stripe phase is

$$H = E_{cl} + \frac{1}{S}\sum_{\vec{k}} A_k(b_k^\dagger b_k + b_{-k}^\dagger b_{-k}) + B_k(b_k^\dagger b_{-k}^\dagger + b_k b_{-k})$$

$$A_k = J_1(1 + \cos k_y) + J_2(1 + \cos\sqrt{3}k_x) + 2K(3 - \cos k_y)$$

$$B_k = -2J_1\left(\cos\frac{\sqrt{3}k_x}{2}\cos\frac{k_y}{2}\right) - 2J_2\left(\cos\frac{\sqrt{3}k_x}{2}\cos\frac{3k_y}{2}\right) - 4K\left(\cos\frac{\sqrt{3}k_x}{2}\cos\frac{k_y}{2}\right).$$

APPENDIX B: HOLSTEIN-PRIMAKOFF TRANSFORMATION FOR NONCOPLANAR CONFIGURATION

In this section, we focus on the system with noncoplanar classical configuration. The spins in the classical configuration is in general $\vec{n} = (\sin\theta\cos\phi, \sin\theta\sin\phi, \cos\theta)$.

If $\theta = 0$, standard Holstein-Primakoff transformation for S is

$$(J_{x0}, J_{y0}, J_{z0}) = \left(\sqrt{2S}\frac{b + b^\dagger}{2}, \sqrt{2S}\frac{b - b^\dagger}{2i}, S - b^\dagger b\right). \tag{B1}$$

Generally, for arbitrary θ and ϕ, we can set

$$J_x = J_{x0} \cos\theta \cos\phi - J_{y0} \sin\phi + J_{z0} \sin\theta \cos\phi$$
$$J_y = J_{x0} \cos\theta \sin\phi + J_{y0} \cos\phi + J_{z0} \sin\theta \sin\phi$$
$$J_z = -J_{x0} \sin\theta + J_{z0} \cos\theta. \tag{B2}$$

Note that commutation relationship and classical extrapolation still holds if we perform the following transformation

$$J_{x0} \rightarrow J_{x0} \cos\alpha + J_{y0} \sin\alpha$$
$$J_{y0} \rightarrow J_{y0} \cos\alpha - J_{x0} \sin\alpha, \tag{B3}$$

which is useful when simplifying the result.

1. Square lattice-CSVC phase

For the classical configuration of CSVC state, the z components of spins follow Neel ordering, while xy components follow SVC ordering. Let the magnitude of the z component be $\cos\phi$, so the xy component has magnitude of $\sin\phi$. By minimizing the classical Hamiltonian, we get

$$\cos^2\phi = \frac{J_1 - 2J_2}{|2K|}. \tag{B4}$$

Here we would like to explicitly write HP transformation for four spins in a square, which corresponds to four sublattices in the system. Spins in the same sublattice should be expressed in the same way.

$$J_i = (J_{z0} \sin\phi + J_{x0} \cos\phi, J_{y0}, J_{z0} \cos\phi - J_{x0} \sin\phi)$$
$$J_j = (J_{y0}, J_{z0} \sin\phi + J_{x0} \cos\phi, -J_{z0} \cos\phi + J_{x0} \sin\phi)$$
$$J_k = (-J_{y0}, -J_{z0} \sin\phi - J_{x0} \cos\phi, -J_{z0} \cos\phi + J_{x0} \sin\phi)$$
$$J_l = (-J_{z0} \sin\phi - J_{x0} \cos\phi, -J_{y0}, J_{z0} \cos\phi - J_{x0} \sin\phi) \tag{B5}$$

Here J_i and J_l are on one diagonal, while J_j and J_k are on the other. The above HP transformation will produce the following translational invariant Hamiltonian, in terms of creation and annihilation operators.

$$H = \frac{1}{S} \sum_{\vec{k}} A_k (b_k^\dagger b_k + b_{-k}^\dagger b_{-k}) + B_k (b_k^\dagger b_{-k}^\dagger + b_k b_{-k}) + \text{const.}$$

$$A_k = (J_1 + 2K \cos^2\phi) \left[2\cos^2\phi - \frac{1}{2} \sin^2\phi (\cos k_x + \cos k_y) \right] + J_2 [2 - 4\cos^2\phi - 2\cos^2\phi \cos k_x \cos k_y]$$
$$\quad - K \sin^2\phi (1 + \cos^2\phi)(2 + \cos k_x + \cos k_y)$$

$$B_k = (J_1 + 2K \cos^2\phi) \left[-\frac{1}{2} \sin^2\phi (\cos k_x + \cos k_y) - i \cos\phi (\cos k_x - \cos k_y) \right] + J_2 [2 \sin^2\phi \cos k_x \cos k_y]$$
$$\quad + K [\sin^4\phi (2 + \cos k_x + \cos k_y) + 2i \sin^2\phi \cos\phi (\cos k_x - \cos k_y)] \tag{B6}$$

One can check that the above A_k and B_k can recover spin wave excitation energy for Neel phase and vortex lattice phase by taking $\phi = 0$ and $\phi = \pi/2$. Note that the classical configuration has four sublattices, so when comparing spin wave excitation energies, we need to fold the Brillouin zone back to $k_x \in [-\pi/2, \pi/2]$, $k_y \in [-\pi/2, \pi/2]$.

2. Triangular lattice-STC phase

For STC state, we decompose the system into four sublattices. HP transformation for spins in the four sublattices is

$$J_i = (x, y, z)$$
$$J_j = (cc'x - cs'z + sy, -cy + sc'x - ss'z, -c'z - s'x)$$
$$J_k = (-c'x + s'z, y, -c'z - s'x)$$
$$J_l = (cc'x - cs'z - sy, -cy - sc'x + ss'z, -c'z - s'x). \tag{B7}$$

Here, (x, y, z) are short for (S_{x0}, S_{y0}, S_{z0}). $c, s = (1/2, \sqrt{3}/2)$ and $(c', s') = (1/3, 2\sqrt{2}/3)$.

The Hamiltonian is

$$
H = \frac{1}{S}\sum_k \Phi \begin{bmatrix} A_k & B_k \\ B_k^\dagger & A_{-k}^* \end{bmatrix} \Phi^\dagger - \frac{4K}{3S}(4N)
$$

$$
\Phi = [b_{1k},\ b_{2k},\ b_{3k},\ b_{4k},\ b_{1-k}^\dagger,\ b_{2-k}^\dagger,\ b_{3-k}^\dagger,\ b_{4-k}^\dagger]
$$

$$
A_k = \left(J_1 + \frac{2}{3}K\right)A_J \circ M_1 + J_2 A_J \circ M_2 - \frac{8K}{9}A_K \circ M_1
$$

$$
B_k = \left(J_1 + \frac{2}{3}K\right)B_J \circ M_1 + J_2 B_J \circ M_2 - \frac{8K}{9}B_K \circ M_1. \tag{B8}
$$

Due to the limit of space, we express A_k and B_k using element-wise product $\circ$. The above 4×4 matrices are

$$
A_J = \begin{bmatrix} 1 & -1/6 + i\sqrt{3}/6 & 1/3 & -1/6 - i\sqrt{3}/6 \\ -1/6 - i\sqrt{3}/6 & 1 & 1/6 + i\sqrt{3}/6 & 1/6 - i\sqrt{3}/6 \\ 1/3 & 1/6 - i\sqrt{3}/6 & 1 & 1/6 + i\sqrt{3}/6 \\ -1/6 + i\sqrt{3}/6 & 1/6 + i\sqrt{3}/6 & 1/6 - i\sqrt{3}/6 & 1 \end{bmatrix}
$$

$$
A_K = \begin{bmatrix} 3 & 1/2 - i\sqrt{3}/2 & -1 & 1/2 + i\sqrt{3}/2 \\ 1/2 + i\sqrt{3}/2 & 3 & -1/2 - i\sqrt{3}/2 & -1/2 + i\sqrt{3}/2 \\ -1 & -1/2 + i\sqrt{3}/2 & 3 & -1/2 - i\sqrt{3}/2 \\ 1/2 - i\sqrt{3}/2 & -1/2 - i\sqrt{3}/2 & -1/2 + i\sqrt{3}/2 & 3 \end{bmatrix}
$$

$$
B_J = \begin{bmatrix} 0 & 1/3 - i\sqrt{3}/3 & -2/3 & 1/3 + i\sqrt{3}/3 \\ 1/3 - i\sqrt{3}/3 & 0 & 2/3 & 2/3 \\ -2/3 & 2/3 & 0 & 2/3 \\ 1/3 + i\sqrt{3}/3 & 2/3 & 2/3 & 0 \end{bmatrix}
$$

$$
B_K = \begin{bmatrix} 0 & 1/2 - i\sqrt{3}/2 & -1 & 1/2 + i\sqrt{3}/2 \\ 1/2 - i\sqrt{3}/2 & 0 & 1 & 1 \\ -1 & 1 & 0 & 1 \\ 1/2 + i\sqrt{3}/2 & 1 & 1 & 0 \end{bmatrix}
$$

$$
M_1 = \frac{1}{2}\begin{bmatrix} 2 & 1 + e^{-i\sqrt{3}k_x + ik_y} & 1 + e^{2ik_y} & 1 + e^{i\sqrt{3}k_x + ik_y} \\ 1 + e^{i\sqrt{3}k_x - ik_y} & 2 & 1 + e^{i\sqrt{3}k_x + ik_y} & e^{i\sqrt{3}k_x + ik_y} + e^{i\sqrt{3}k_x - ik_y} \\ 1 + e^{-2ik_y} & 1 + e^{-i\sqrt{3}k_x - ik_y} & 2 & 1 + e^{i\sqrt{3}k_x - ik_y} \\ 1 + e^{-i\sqrt{3}k_x - ik_y} & e^{-i\sqrt{3}k_x - ik_y} + e^{-i\sqrt{3}k_x + ik_y} & 1 + e^{-i\sqrt{3}k_x + ik_y} & 2 \end{bmatrix}
$$

$$
M_2 = \frac{1}{2}\begin{bmatrix} 2 & e^{-i\sqrt{3}k_x - ik_y} + e^{2ik_y} & e^{-i\sqrt{3}k_x + ik_y} + e^{i\sqrt{3}k_x + ik_y} & e^{i\sqrt{3}k_x - ik_y} + e^{2ik_y} \\ e^{i\sqrt{3}k_x + ik_y} + e^{-2ik_y} & 2 & e^{i\sqrt{3}k_x - ik_y} + e^{2ik_y} & 1 + e^{2i\sqrt{3}k_x} \\ e^{i\sqrt{3}k_x - ik_y} + e^{-i\sqrt{3}k_x - ik_y} & e^{-i\sqrt{3}k_x + ik_y} + e^{-2ik_y} & 2 & e^{i\sqrt{3}k_x + ik_y} + e^{-2ik_y} \\ e^{-i\sqrt{3}k_x + ik_y} + e^{-2ik_y} & 1 + e^{-2i\sqrt{3}k_x} & e^{-i\sqrt{3}k_x - ik_y} + e^{2ik_y} & 2 \end{bmatrix}. \tag{B9}
$$

The Hamiltonian can then be diagonalized using standard Bogoliubov transformation.

APPENDIX C: SQUARE LATTICE-NEMATIC AND SNVC AND CHIRAL PHASE

Let us first consider SNVC phase. Without loss of generality, let us consider S_i along x and $S_{i+\hat{x}}$ along z. The cross product is then $(YZ + XY, -XX - ZZ, ZY - YX)$. Here letter X is short for S_{x0}, and we keep the first letter for S_i and second letter for $S_{i+\hat{x}}$. Now we can plug in HP transformation. After summing over site i, only the second component of the cross product is nonzero, since x and z components contain integration of odd function of k_x. The result is

$$
\mathcal{S}_{\text{SNVC}} = \sum_{\vec{k}} \left(2 - \frac{\cos(k_x) + \cos(k_y)}{2}\right)v_k^2 + \left(-\frac{\cos(k_x) + \cos(k_y)}{2}\right)u_k v_k
$$

$$
v_k^2 = \frac{1}{2}\left(\frac{|A_k|}{\sqrt{A_k^2 - B_k^2}} - 1\right)
$$

$$
u_k v_k = -\frac{1}{2}\frac{B_k}{\sqrt{A_k^2 - B_k^2}}\text{sign}(A_k). \tag{C1}
$$

For the chiral state, we can perform the same calculation. We first write order parameter in terms of $S_{x0,y0,z0}$ and then plug in HP transformation. Eventually we sum up all sites. The result is

$$\mathcal{S}_{\text{chir}} = \frac{1}{\cos\phi} \sum_{\vec{k}} \left[3\cos\phi - \cos\phi\cos(k_x - k_y) + \frac{1}{2}(\cos k_x + \cos k_y) \right] v_k^2 + \left[\cos\phi\cos(k_x - k_y) + \frac{1}{2}(\cos k_x + \cos k_y) \right] u_k v_k.$$

(C2)

[1] C. Broholm, R. J. Cava, S. A. Kivelson, D. G. Nocera, M. R. Norman, and T. Senthil, Science **367**, eaay0668 (2020).

[2] F. Wang, S. A. Kivelson, and D.-H. Lee, Nat. Phys. **11**, 959 (2015).

[3] J. Chayes, L. Chayes, and S. Kivelson, Commun. Math. Phys. **123**, 53 (1989).

[4] C. Xu, M. Müller, and S. Sachdev, Phys. Rev. B **78**, 020501(R) (2008).

[5] R. M. Fernandes, S. A. Kivelson, and E. Berg, Phys. Rev. B **93**, 014511 (2016).

[6] R. M. Fernandes, A. V. Chubukov, and J. Schmalian, Nat. Phys. **10**, 97 (2014).

[7] A. V. Chubukov, R. M. Fernandes, and J. Schmalian, Phys. Rev. B **91**, 201105(R) (2015).

[8] H. C. Jiang, F. Krüger, J. E. Moore, D. N. Sheng, J. Zaanen, and Z. Y. Weng, Phys. Rev. B **79**, 174409 (2009).

[9] H.-C. Jiang, H. Yao, and L. Balents, Phys. Rev. B **86**, 024424 (2012).

[10] F. Figueirido, A. Karlhede, S. Kivelson, S. Sondhi, M. Rocek, and D. S. Rokhsar, Phys. Rev. B **41**, 4619 (1990).

[11] J. Richter, R. Zinke, and D. J. Farnell, Eur. Phys. J. B **88**, 2 (2015).

[12] S.-S. Gong, W. Zhu, D. N. Sheng, O. I. Motrunich, and M. P. A. Fisher, Phys. Rev. Lett. **113**, 027201 (2014).

[13] L. Capriotti, F. Becca, A. Parola, and S. Sorella, Phys. Rev. Lett. **87**, 097201 (2001).

[14] Y. Iqbal, P. Ghosh, R. Narayanan, B. Kumar, J. Reuther, and R. Thomale, Phys. Rev. B **94**, 224403 (2016).

[15] W.-J. Hu, F. Becca, A. Parola, and S. Sorella, Phys. Rev. B **88**, 060402(R) (2013).

[16] T. Li, F. Becca, W. Hu, and S. Sorella, Phys. Rev. B **86**, 075111 (2012).

[17] S. Morita, R. Kaneko, and M. Imada, J. Phys. Soc. Jpn. **84**, 024720 (2015).

[18] L. Wang, Z.-C. Gu, F. Verstraete, and X.-G. Wen, Phys. Rev. B **94**, 075143 (2016).

[19] Y. Iqbal, W.-J. Hu, R. Thomale, D. Poilblanc, and F. Becca, Phys. Rev. B **93**, 144411 (2016).

[20] W.-J. Hu, S.-S. Gong, W. Zhu, and D. N. Sheng, Phys. Rev. B **92**, 140403(R) (2015).

[21] R. Kaneko, S. Morita, and M. Imada, J. Phys. Soc. Jpn. **83**, 093707 (2014).

[22] Z. Zhu and S. R. White, Phys. Rev. B **92**, 041105(R) (2015).

[23] P. Chandra, P. Coleman, and A. I. Larkin, Phys. Rev. Lett. **64**, 88 (1990).

[24] Q. Zhong and S. Sorella, Europhys. Lett. **21**, 629 (1993).

[25] A. V. Chubukov and T. Jolicoeur, Phys. Rev. B **46**, 11137 (1992).

[26] L. X. Hayden, T. A. Kaplan, and S. D. Mahanti, Phys. Rev. Lett. **105**, 047203 (2010).

[27] P. Chandra and B. Doucot, Phys. Rev. B **38**, 9335 (1988).

[28] C. Fang, H. Yao, W.-F. Tsai, J. P. Hu, and S. A. Kivelson, Phys. Rev. B **77**, 224509 (2008).

[29] C. Luo, T. Datta, and D.-X. Yao, Phys. Rev. B **93**, 235148 (2016).

[30] D. Stanek, O. P. Sushkov, and G. S. Uhrig, Phys. Rev. B **84**, 064505 (2011).

[31] M. Ye and A. V. Chubukov, Phys. Rev. B **95**, 014425 (2017).

[32] A. L. Chernyshev and M. E. Zhitomirsky, Phys. Rev. B **79**, 144416 (2009).

[33] G. E. Castilla and S. Chakravarty, Phys. Rev. B **43**, 13687 (1991).

[34] L. Nie, G. Tarjus, and S. A. Kivelson, Proc. Natl. Acad. Sci. **111**, 7980 (2014).

[35] C.-H. Hsu, S. Raghu, and S. Chakravarty, Phys. Rev. B **84**, 155111 (2011).

[36] T. Senthil, A. Vishwanath, L. Balents, S. Sachdev, and M. P. Fisher, Science **303**, 1490 (2004).

[37] B. E. Larson and C. L. Henley, Effective hamiltonians for state selection in heisenberg antiferromagnets, arXiv:0811.0955.

[38] K. Majumdar, Phys. Rev. B **82**, 144407 (2010).

[39] S. Chakravarty, B. I. Halperin, and D. R. Nelson, Phys. Rev. B **39**, 2344 (1989).

[40] F. D. M. Haldane, Phys. Rev. Lett. **61**, 1029 (1988).

[41] N. Read and S. Sachdev, Phys. Rev. Lett. **62**, 1694 (1989).

[42] T. Senthil and M. P. A. Fisher, Phys. Rev. B **74**, 064405 (2006).

[43] I. Affleck, T. Kennedy, E. H. Lieb, and H. Tasaki, *Condensed Matter Physics and Exactly Soluble Models* (Springer, Berlin, Germany, 2004), pp. 249–252.

[44] E. Lieb, T. Schultz, and D. Mattis, Ann. Phys. **16**, 407 (1961).

[45] M. Yamanaka, M. Oshikawa, and I. Affleck, in *APS March Meeting Abstracts* (1997).

[46] M. B. Hastings, Phys. Rev. B **69**, 104431 (2004).

[47] R. Haghshenas, W.-W. Lan, S.-S. Gong, and D. N. Sheng, Phys. Rev. B **97**, 184436 (2018).

[48] R. F. Bishop, P. H. Y. Li, R. Darradi, and J. Richter, Europhys. Lett. **83**, 47004 (2008).